Proceedings of the 2009 IEEE
International Conference on Robotics and Biomimetics
December 19 -23, 2009, Guilin, China

Improvement of Redundant Manipulator Task Agility Using Multiobjective Weighted Isotropy-Based Placement Optimization

Frank L. Hammond III, and Kenji Shimada, *Member, IEEE*

***Abstract*—The measurement and improvement of task agility, the ability of a manipulator to effectively handle multiple task types, has become increasingly important in the manufacturing industry as efforts are made to design more versatile and efficient factories. Task agility is crucial to the performance of kinematically redundant manipulators in complex manufacturing workspaces that involve several physical motion impediments and conservative dynamic actuation constraints, and which are used to complete a wide variety of manufacturing operations. Manipulator morphology and workspace layout optimizations offer robust, long term solutions to the problem of improving task agility, but the cost of redevelopment or redeployment is typically prohibitive. Manipulator placement optimization is a more economically feasible and practical solution that is amenable to short term implementation.**

In this paper we propose the use of a multiobjective weighted isotropy measure as a task agility metric and submit it as the basis for optimizing the placement of redundant manipulators in a complex, multitask workspaces. We describe the formulation of this measure, how it factors motion impedance into kinematic dexterity, and the advantages of this measure over previous task agility measurement methods. We demonstrate its efficacy in improving task agility by optimizing manipulator base placement to achieve collision-free motion and reduced maximum torques across an entire set of disparate manipulation tasks.

Index Terms – Inverse kinematics, inverse dynamics, redundant, kinematic isotropy, task agility

I. Introduction

Most modern manufacturing workspaces contain several physical obstacles such as workspace boundaries, production parts, part feeders, and, in the case of cooperative tasks, assistive robots that constrain manipulator motion (Fig. 1). The virtual motion impediments of dynamic actuation limitations, such as maximum torque and acceleration, and kinematic motion ranges also impose constraints on manipulator motion. These motion impediments, while inherent in every manufacturing system, serve to limit the performance and versatility, or task agility, of the associated manipulators and must be removed or sufficiently reduced to increase workspace efficiency.

Manuscript received on July 31, 2009; revised October 9, 2009. Frank L. Hammond III is with the Department of Mechanical Engineering, Carnegie Mellon University, 5000 Forbes Avenue, Pittsburgh, PA 15213 USA (phone: 215-882-4493; fax: 412-268-3348; e-mail: fhammond@ cmu.edu).

Kenji Shimada., is with the Department of Mechanical Engineering, Carnegie Mellon University, 5000 Forbes Avenue, Pittsburgh, PA 15213 USA (e-mail: shimada@cmu.edu).

The aforementioned physical motion impediments are essential to the completion of manufacturing tasks and, with the exception of the assistive manipulators, cannot easily be moved or reconfigured within the workspace. The virtual impediments, while mitigable by motion planning methods, are heavily dependent upon placement and morphology. The task-specific morphological design of more suitable manipulators can provide robust, long term solutions to the problem of increasing task agility, but is often a costly, sometimes economically prohibitive process. As such, the less costly, more easily implemented manipulator placement optimization is the often the preferred method of task agility improvement.

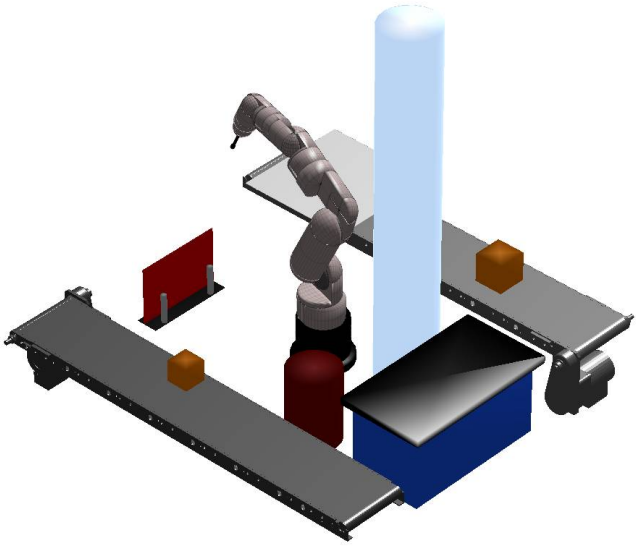

Fig. 1. A multitask workspace that contains enough equipment and parts to perform several different tasks. The 8DOF manipulator (center) must be placed such that all tasks can be performed without incidence of collision, torque limit violation, and loss of dexterity or reach, all while adhering the task motion and timing specifications.

The selection of a treatment for manipulator placement optimization and the performance metrics by which design fitness is measured depends upon the context in which optimality is defined and the intended performance goals. High throughput pick-and-place tasks require manipulator placements that maximize motion velocity and hasten task completion, and this can be achieved by optimizing over cycle time [1] or kinematic manipulability [2]. Low throughput, heavy duty tasks require placements that increase mechanical advantage and promote low torque and energy consumption, and optimizing over dynamic manipulability [3], energy, or torque can address this.

978-1-4244-4775-6/09/$25.00 ©

Workspaces containing several obstacles require placements conducive to collision avoidance, and this can be achieved by optimizing over minimum obstacle distance. Time-varying and multitask workspaces require a combination these requirements, and thus call for performance measures that encompass both kinematic and dynamic motion resistances and which can be used to evaluate performance over multiple tasks. Such measures were recently developed by the authors and are used here as the basis for optimizing manipulator placement to achieve competing performance objectives of speed, mechanical power, and collision avoidance while negotiating the motion impedances they impose [4, 5].

Section II of this paper discusses previous work on manipulator optimization and placement, including the authors' development weighted isotropy measures, and explains the concept of multiobjective weighted isotropy, the main contribution of this paper. Section III describes the multitask workspace and the set of tasks over which manipulator base position is optimized to improve task agility. Section IV examines the results from the task-specific manipulator placement optimization and Section V discusses the implications of improved task agility on the adaptability of a manipulator to new tasks or environments.

II. Related Work

A. Previous Approaches to Placement Optimization

The problem of manipulator placement optimization is a classical, well-studied one that is often encountered in factory workcell layouts. The problem of improving task agility to design highly flexible manufacturing systems is a more recent challenge but has been addressed using several different manipulator placement methods. Due to the non-linearity of manipulator kinematics and dynamics, especially in the redundant case, and path planning algorithms, and the sheer size and complexity of manufacturing workspaces and tasks, a majority of these methodologies are heuristic in nature and involve the optimization of manipulator placement over a set of performance measures.

Pamanes and Zeghloul [6] define optimality using a normalized set of the disparate kinematic modalities of kinematic manipulability, joint limitations, and Jacobian condition number. Lueth [7] employs a combination a reachable workspace computation, collision avoidance, and path planning to optimize manipulator placement in a workcell layout for a collision-free minimum distance motion path. Pashkevich and Pashkevich [8] optimize manipulator placement over kinematic and dynamic manipulability, cycle time, and distance to joint limits using genetic algorithms (GAs). Hsu, Latombe, and Sorkin [9] use a two-step optimization algorithm consists of a randomized path planning and manipulator base relocation to determine the best placement for a minimum-time collision-free path.

Each of the methods yield near-optimal placements for individual tasks with respect to the specified performance measures but inherently lacks the capacity to consider multiple tasks or workspaces or to comprehensively measure kinematic and dynamic fitness. This is due, in part, to the limitations of the performance metrics, particularly the dexterity measures being used.

B. Kinematic Dexterity Measures

Most dexterity measures do not give explicit information about the cycle time, maximum torque and energy, or collision avoidance capability of a manipulator as they relate to its placement, but they are generally appropriate for measuring smoothness of motion and the balance of kinematic and dynamics performance. One of the earliest proposed and most well-recognized proposed Jacobian-based manipulator performance metrics was Yoshikawa's scalar manipulability index μ [2], shown here,

$$\mu = \sqrt{\det\left(\mathbf{J}(\boldsymbol{\theta})\mathbf{J}(\boldsymbol{\theta})^T\right)}, \qquad (1)$$

which quantifies local dexterity for serial manipulators as a function of an instantaneous joint position vector $\boldsymbol{\theta}$. The manipulability index has proven effective when measuring and optimizing motion smoothness and avoiding kinematic singularities. Unfortunately, because derived using only the manipulator Jacobian matrix, it suffers from scale, order, and dimensional homogeneity dependencies that prevent an accurate comparison of performance between two or more competing morphologies.

Several more recently developed dexterity metrics remove these dependencies from Jacobian-based performance measurement in order in facilitate comparison of performance between different manipulator types, which is a requisite for motion control and design optimization. Klein and Blaho [10] use the matrix condition number to eliminate dimensional dependencies. Stocco, Salcudean and Sassani [11], Khan and Angeles [12], and Tandirci, Angeles and Ranjbaran [13], normalize the Jacobian and eliminate heterogeneity, due in part to the simultaneous use of linear and rotary actuators, by factoring the "characteristic length" out of the manipulator Jacobian. Kim and Khosla [14] defined a measure of dexterity called the measure of isotropy, shown here

$$\Delta = \frac{M}{\Psi} = \frac{\left(\sqrt[m]{\det\left(\mathbf{J}(\boldsymbol{\theta})\mathbf{J}(\boldsymbol{\theta})^T\right)}\right)}{\left(\frac{\mathrm{trace}(\mathbf{J}(\boldsymbol{\theta})\mathbf{J}(\boldsymbol{\theta})^T)}{\mathrm{order}\ m}\right)} \qquad (2)$$

which factors both scale and order dependency from the Jacobian using the arithmetic eigenvalue mean Ψ, and the order-independent manipulability, or geometric mean, M.

The previously mentioned kinematic dexterity metrics are local measures of performance which are dependent upon the current operating point and manipulator posture, given by joint position vector $\boldsymbol{\theta}$. Stocco, Salcudean and Sassani [11] proposed a more comprehensive measure called the Global Isotropy Index (*GII*), which takes the ratio of the smallest and largest singular values, σ_{min} and σ_{max} of the manipulator Jacobian matrix over the entire workspace

W_{space}. Here, x is the manipulator end-effector position and p is the robot base location within the workspace.

$$GII(p) = \max_{x \in W_{space}} \min \frac{\sigma_{\min}(\mathbf{J}(\boldsymbol{\theta}, x))}{\sigma_{\max}(\mathbf{J}(\boldsymbol{\theta}, x))}. \quad (3)$$

The GII provides adequate information about the global dexterity of a manipulator across a set of tasks or a workspace, but does not consider collision avoidance and dynamic actuation limits which are necessary for multiobjective optimization.

C. Collision Avoidance-Weighted Dexterity Measure

Recently, Hammond and Shimada [4] proposed the modification of the *GII* and Δ to account for the motion limits imposed by workspace obstacles by scaling the manipulator Jacobian with an n x n diagonal weighting matrix **W**, defined here

$$\mathbf{W}(\dot{\boldsymbol{\theta}}, \xi) = \begin{bmatrix} w_1 & 0 & 0 \\ 0 & \ddots & 0 \\ 0 & 0 & w_n \end{bmatrix}. \quad (4)$$

This matrix factors the effect of physical motion impediments into the isotropy measure by penalizing joint transmission rates when, and only when, joint motion causes movement toward undesired contact with the environment. Each diagonal element w_i in matrix **W**, defined here,

$$w_i = \alpha \left[(1-\beta)\left(1 + e^{\left(\|\dot{\theta}_i - \xi_i\|\right)}\right)^{-1} + \beta \right], \quad (5)$$

is a sigmoid function of instantaneous kinematic joint velocity $\boldsymbol{\theta}_i$, due to task trajectory goals, and an obstacle avoidance joint velocity $\boldsymbol{\xi}_i$, where the subscript i denotes the joint number. Variable α is a proximity factor that decreases from 1 to 0 as minimum obstacle distance falls below some critical distance, and β is a value between 1 and 0 that limits the isotropy penalty incurred for motion impedances.

The avoidance-weighted global isotropy index (AWGII), is written as,

$$AWGII = \max_{x \in \mathbf{W}_{space}} \min \frac{\sqrt{\sigma_{\min}(\mathbf{J}(\boldsymbol{\theta})\mathbf{W}(\dot{\boldsymbol{\theta}}, \xi)\mathbf{J}(\boldsymbol{\theta})^T)}}{\sqrt{\sigma_{\max}(\mathbf{J}(\boldsymbol{\theta})\mathbf{W}(\dot{\boldsymbol{\theta}}, \xi)\mathbf{J}(\boldsymbol{\theta})^T)}} \quad (6)$$

which is equivalent to taking the singular values of the Jacobian itself. When no obstacle-related motion penalties are incurred, the weight matrix becomes an identity matrix and the resulting ratio is identical to the one obtained using the GII calculation (3).

The obstacle avoidance joint velocities [15] used in forming the weight matrix are calculated by mapping task-space avoidance vectors onto the kinematic null space (7).

$$\dot{\boldsymbol{\theta}} = \mathbf{J}^{+}\dot{\mathbf{x}} + \sum_{i=1}^{n}\left(\alpha_{\eta i}\left[\mathbf{J}_o\left(\mathbf{I} - \mathbf{J}_e^{+}\mathbf{J}_e\right)\right]^{+}\left(\alpha_{oi}\dot{\mathbf{x}}_{oi} - \mathbf{J}_o\mathbf{J}_e^{+}\dot{\mathbf{x}}_e\right)\right) \quad (7)$$

where $\mathbf{J}_e$ is the end-effector Jacobian, $\mathbf{J}_{oi}$ is the obstacle point Jacobian for the ith obstacle, x_{oi} is the task-space avoidance velocity, and $\alpha_{\eta i}$ and α_{oi} are the gain term and the avoidance velocity magnitude the ith obstacle, respectively.

D. Torque Weighted Dexterity Measure

Hammond and Shimada [5] also proposed the modification of the GII to account for joint torque limits is a done using the same technique used for obstacle avoidance, only now an n x n diagonal torque-weighting matrix **T**, defined in Equation (8), is employed.

$$\mathbf{T}(\boldsymbol{\tau}, \boldsymbol{\tau}_{\max}) = \begin{bmatrix} t_1 & 0 & 0 \\ 0 & \ddots & 0 \\ 0 & 0 & t_n \end{bmatrix} \quad (8)$$

This matrix decreases the transmission of joint velocities to task space velocities if joint motion results `in excessive torque. Each element t_i in matrix **T**, defined here

$$t_i = 1 - \lambda^{-\eta(\tau_{\max} - \|\tau_i\|)} \quad (9)$$

is a non-linear function of the instantaneous joint torque τ_i and maximum torque rating τ_{max}. Variable λ is an arbitrary scalar value between 0 and 1 which determines the maximum joint transmission penalty incurred when joint torque τ_i approaches τ_{max}, while η determines the function curvature, of rate of penalty increase.

The weights t_i in matrix **T** are exponentially proportional to the distance of joint torque τ_i from maximum joint torque τ_{max}, also called the torque clearance. This relationship penalizes all motions that require torques near or beyond safety limits, and, by extension, penalizes all manipulator morphologies or placements which lead to these motions. Figure 1 illustrates the penalty function behavior with respect to percentage of maximum torque rating.

The torque-weighted global isotropy index (TWGII) written as,

$$TWGII = \max_{\mathbf{W}_{space}} \min \frac{\sqrt{\sigma_{\min}(\mathbf{J}(\boldsymbol{\theta})\mathbf{T}(\boldsymbol{\tau}, \boldsymbol{\tau}_{\max})\mathbf{J}(\boldsymbol{\theta})^T)}}{\sqrt{\sigma_{\max}(\mathbf{J}(\boldsymbol{\theta})\mathbf{T}(\boldsymbol{\tau}, \boldsymbol{\tau}_{\max})\mathbf{J}(\boldsymbol{\theta})^T)}}. \quad (10)$$

When the torque-weighted matrix is an identity matrix, which is the case when no torque-related motion penalties are incurred, this ratio is identical to the one obtained using equation (3).

The joint torques used in the formulation of the torque-weighting matrix **T** are calculated with the recursive Newton-Euler method [16]. The fundamental Newton-Euler method equation, shown here

$$\boldsymbol{\tau} = \mathbf{H}(\dot{\boldsymbol{\theta}})\ddot{\boldsymbol{\theta}} + \mathbf{C}(\boldsymbol{\theta}, \dot{\boldsymbol{\theta}}) + \mathbf{g} + \mathbf{F} \quad (11)$$

consists of an inertia matrix **H**, a Coriolis-centrifugal force vector **C**, and gravitational and external force vectors **g** and **F**. Both **H** and **C** are functions of joint position and velocity, and play important roles in the calculation of energy consumption and in motion control methods that minimize local torque requirements.

E. Multiobjective Weighted Dexterity Measure

In this study, manipulator placement optimality is a function of both obstacle avoidance capability and torque limitation. The aforementioned weighting techniques are sufficient to address either one of these two design optimization goals individually but when considering both goals simultaneously, the weighing functions must be combined in a way the preserves their functionality. We combine the functions by taking the product of the obstacle avoidance-weighting matrix **W** and torque-weighting matrix **T** to get multi-objective weighting matrix **M**, as shown in equation (12).

$$\mathbf{M}(\dot{\boldsymbol{\theta}},\boldsymbol{\xi},\boldsymbol{\tau},\boldsymbol{\tau}_{\max}) = \mathbf{W}(\dot{\boldsymbol{\theta}},\boldsymbol{\xi})\cdot\mathbf{T}(\boldsymbol{\tau},\boldsymbol{\tau}_{\max}) = \begin{bmatrix} m_1 & 0 & 0 \\ 0 & \ddots & 0 \\ 0 & 0 & m_n \end{bmatrix} \quad (12)$$

Here, each element m_i is the product of elements t_i and w_i from weighting matrices **T** and **W**, respectively. Following the formulation used to weight the GII in the previous sections, we create the multi-objective global isotropy index (MWGII) as shown in equation (13).

$$MWGII = \max_{\mathbf{W}_{space}} \min \frac{\sqrt{\sigma_{\min}(\mathbf{J}(\boldsymbol{\theta})\mathbf{M}(\dot{\boldsymbol{\theta}},\boldsymbol{\xi},\boldsymbol{\tau},\boldsymbol{\tau}_{\max})\mathbf{J}(\boldsymbol{\theta})^T)}}{\sqrt{\sigma_{\max}(\mathbf{J}(\boldsymbol{\theta})\mathbf{M}(\dot{\boldsymbol{\theta}},\boldsymbol{\xi},\boldsymbol{\tau},\boldsymbol{\tau}_{\max})\mathbf{J}(\boldsymbol{\theta})^T)}} \quad (13)$$

III. Manipulator Placement Optimization

A. Definition of Manipulator Placement Fitness

The optimality of manipulator placement is specific to the context of the application and the performance demands on the robot, and can be measured by various metrics, each with its own implications on performance improvement. In this case we are optimizing the placement of an eight degree-of-freedom (8-DOF) manipulator over an obstacle-laden, multitask workspace while performing tasks that test dynamic actuation limits. Thus our goal is to take into account the effect of motion impediments on dexterity while maintaining low torque levels, relative to torque limits, and maximizing kinematic isotropy. Here, the optimal manipulator placement is defined as that which maximizes the MWGII over the entire set of tasks for the given workspaces.

B. Manipulator Structure and Actuation Specifications

The manipulator morphology used in this optimization study was borrowed from an 8-DOF prototype industrial robot design. The DH parameters for the transformations representing the kinematic structure of the manipulator are listed in Table I, and a plot of the morphology, generated using the authors' software, is shown in Fig. 2.

TABLE I
8DOF Manipulator Denavit-Hartenberg (DH) Parameters

Link	a_i(mm)	α_i(°)	d_i(mm)	θ_i(°)	τ_{maxn} (N·m)
1	40	-90	300	θ_1	2000
2	450	75	0	θ_2+90	2400
3	150	0	0	θ_3+90	2200
4	0	-90	525	θ_4	1200
5	0	-90	0	θ_5+90	1000
6	0	-90	450	θ_6	800
7	0	-90	0	θ_7	700
8	0	0	270	θ_8	250

The four Denavit-Hartenberg parameters are link length a_i, link twist angle α_i, link offset d_i and joint angle θ_i. The dynamic actuation specification is the maximum torque τ_{max}.

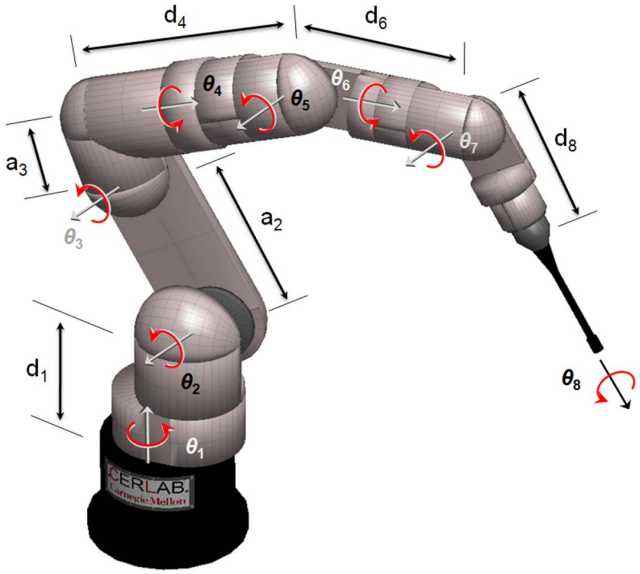

Fig. 2. A plot showing the major physical dimensions of the 8DOF manipulator and the locations of the eight revolute joints comprising it.

C. Workspace and Task Specifications

The multitask workspace spans a square floor space 3000 mm x 3000 mm in dimension and has a height of 2000 mm. The manipulator is initially located at the center of the workspace, at coordinate [x,y,z] = [0,0,0] mm, as shown in Fig. 3.

There are four different tasks that the 8DOF manipulator performs, each task having its own group of workspace equipment, task objects or parts to be manipulated, and motion path control points. Each of these tasks was designed to test efficacy of the MWGII in achieving a placement conducive the collision avoidance, torque limit avoidance and energy minimization, and kinematic isotropy.

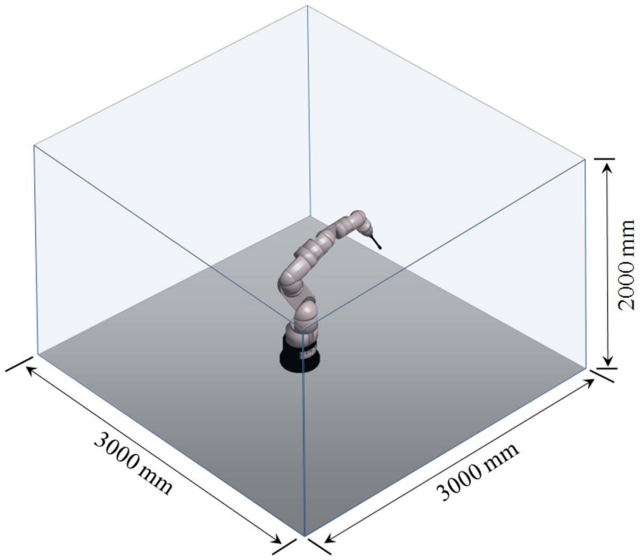

Fig. 3. The dimensions of the multitask workspace and the location of the 8DOF manipulator at its center.

The box lifting task, shown in Fig. 4, consists of lifting a 10kg box from a conveyor belt and placing it onto a workstation table. This task is required to have a cycle time for 4.0 seconds and must not cause excessive manipulator torques. It is designed to test the MWGII's ability to balance of high torques created by speed requirements while finding a placement location conducive to kinematic isotropy.

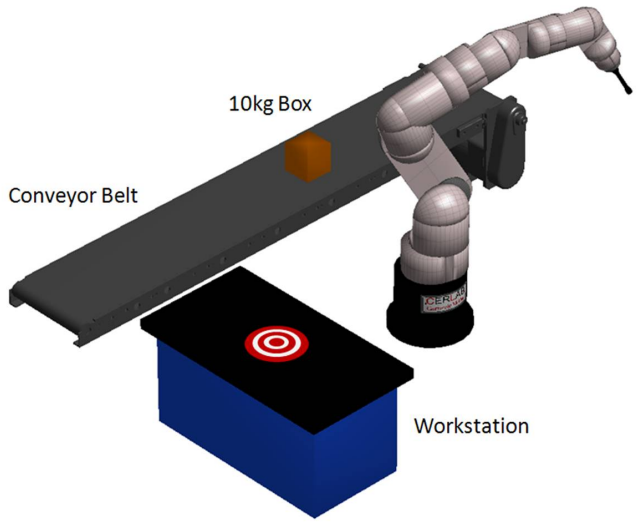

Fig. 4. The layout of the workspace during the box lift task.

The plate moving task, shown in Fig. 5, consists of lifting a 150kg steel plate from the conveyors and placing it on its side in a plate stacking brace. This task has a cycle time of 8.0 seconds and must not cause collisions between the plate and other workspace equipment. It is designed to test the MWGII's efficacy in preventing excessive torques that might damage joint actuators.

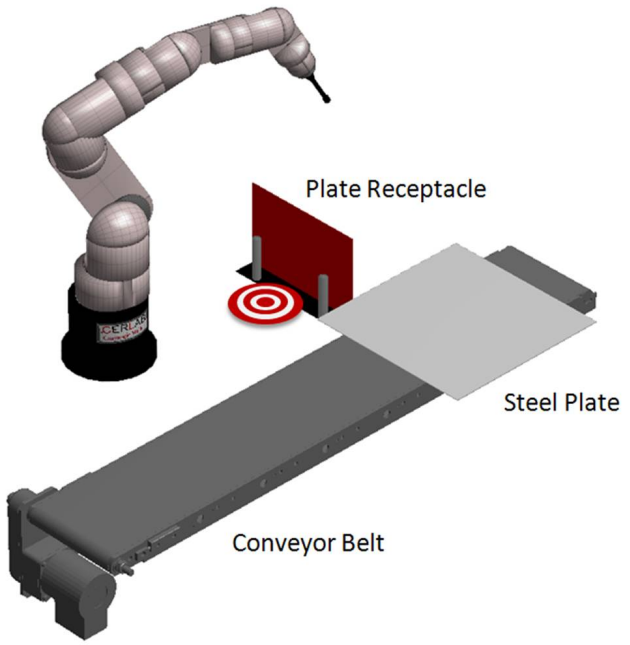

Fig. 5. The layout of the workspace during the plate moving task.

The column avoidance task, shown in Fig. 6, consists of reaching around an ill-placed weight-bearing structure, retrieving a 20kg package from a conveyor, and placing the package onto the workstation. This task has a cycle time of 6.0 seconds and requires that the manipulator and its payload never come in contact with the column. It is designed explictly to test obstacle avoidance.

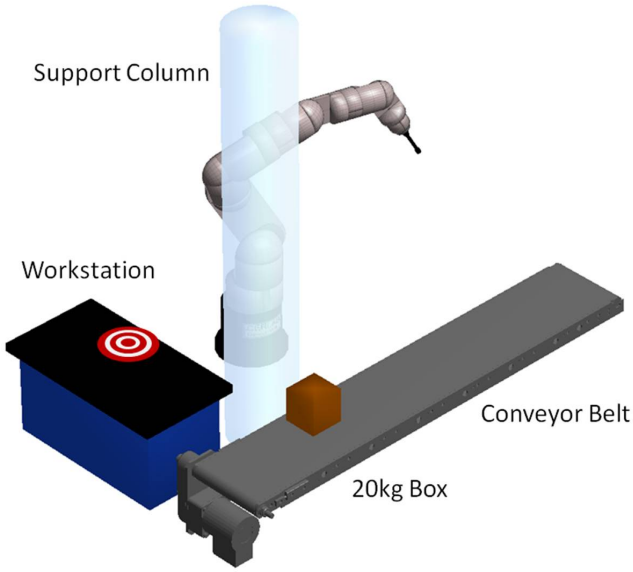

Fig. 6. The layout of the workspace during the column avoidance task

The barrel manipulation task, shown in Fig. 7, calls of the lifting of a 75kg barrell from the floor of the workspace space and placing it on its side into a workstation, then placing it, by its top, onto a pallet. It has a cycle time a 15.0 seconds and is designed to test torque limit avoidance while maitaining high dexterity.

These tasks and cycle times were chosen based upon several observed small-scale manufacturing workcells and have been configured to better represent the large disparity in task requirements and workspace types that we intend optimize manipulator placements for. The authors understand that this task set is one not likely to be found in a typical industrial manufacturing setting but nonetheless find it to be suitable for demonstration of the improvement in task agility that can be achieved using the MWGII.

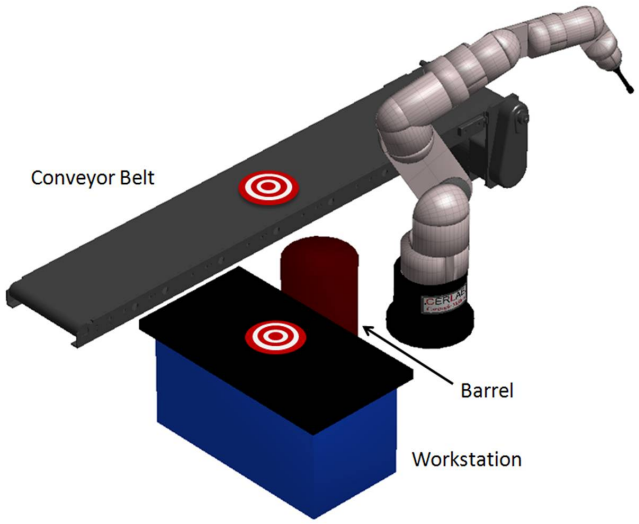

Fig. 7. The layout of the workspace during the barrel lift task.

A top-down view of the multitask workspace is shown in Fig. 8. The dimensions and center point locations for each workspace component are shown in Table II.

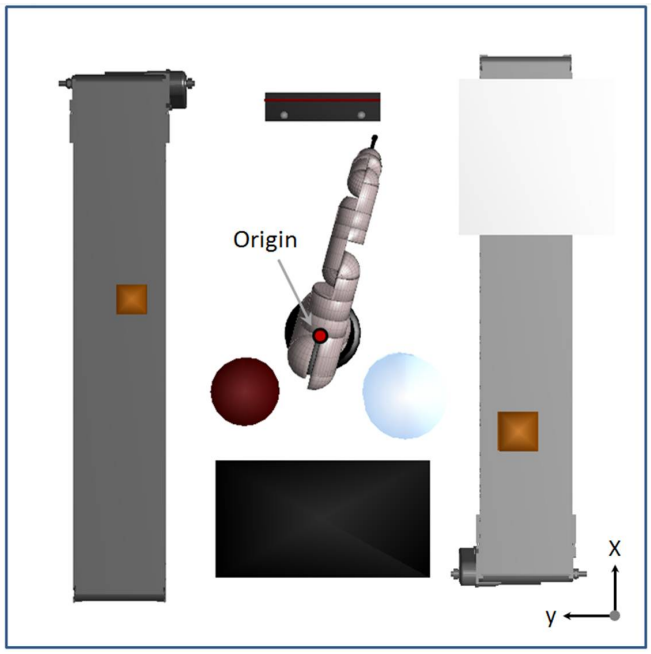

Fig. 8. Top-down view of the entire multitask workspace. Dimensions and locations of workspace components are listed in Table II.

TABLE II
WORKSPACE COMPONENT DIMENSIONS AND LOCATIONS

Component	Size *(l,w,h)* (mm)	Location *(x,y,z)* (mm)
10kg box	150,150,150	100,900,500
20kg box	200,200,200	100,-1000,500
Steel plate	800,800,10	300,-1200,500
Barrel	500(h),350(d)	-500,400,0
Conveyor 1	2800,490,500	0,1000,0
Conveyor 2	2800,490,500	0,-1000,0
Workstation	1000,500,500	-1000,0,0
Plate Brace	600,150,300	900,0,0
Column	2000(h),300(d)	-300,400,0

Dimensions and locations of multitask workspace components.

D. Optimization Method

The optimization of the 8DOF manipulator placement involved three steps:

1. Defining placement optimization search area
2. Simulate the manipulator performing all four tasks at each candidate placement
3. Using a nonlinear constrained optimization, converge to the placement with the highest MWGII value.

The placement optimization search was configured to cover all feasible workspace placements. The z-coordinate of the manipulator was fixed, at zero.

The motion for each task consisted only a single object retrieval point, a maximum of 3 motion points, and one placement point. The intermediate motion points were determined by inverse kinematics and dynamics, and collision avoidance [14], and were interpolated to result in the specified cycle times. Joint actuator torques were minimized locally using inertia-matrix based control methods [17]. A damped least squares pseudoinverse formulation was used to solve for inverse kinematics and trace the task trajectory while avoiding singularity configurations [18,19]. Joint limitations were enforced using a motion penalty function [20] to ensure that all solution postures were mechanically feasible.

The nonlinear optimization search was conducted using the MATLAB Optimization Toolbox. The FMINCON search was configured to use finite-difference center derivatives to solve for the MWGII gradient at each candidate placement, and the stopping criteria were set to a function tolerance of 10^{-15} and a maximum iteration count of 1000. The step size in the search algorithm was allowed to range from 0.001mm to 50mm, depending upon the size of the gradient at each step.

Several performance metrics, including individual joint torque, global isotropy, and, the focus of this study, MGWII, were recorded during each simulation of all four tasks at each candidate manipulator placement. The overall fitness of a morphology for the given manipulation task was determined from these metrics. The objective function to be maximized is the MWGII.

E. Selection of MWGII Parameters

The MWGII, which is comprised of the AGWII and TWGII, has a total of four parameters associated with its penalty functions. For the AGWII penalty function, α is set to 1.0 and β is set to 0.75. These settings limit the joint transmission ratio penalty to 75% of the normal value. For the TWGII penalty function, λ is set to 1.0 and η is set to 5. These settings allow a joint transmission ratio penalty of 100% if torque exceeds the maximum, and shapes the function such that the 50% penalty occurs when torque is approximately 85% of the maximum.

IV. Base Placement Optimization Results

A. MWGII-based Kinematic Fitness Results

The manipulation optimization placement search yielded a maximum MWGII value of 0.0389 at [x,y] = [-21.5,-20.5], shown by contour plot in Fig. 9, after 704 iterations. This location, according to the MWGII, is the placement that best balances collision avoidance and torque limit adherence, as they relate to kinematic isotropy, over the entire task set. The optimal placement does not result in minimum total energy consumption (by limiting torque) or optimum global isotropy as achieving either of these opposing goals would naturally yield suboptimal, if not poor, performance on the other. This would likely serve to decrease the task agility of the manipulator because it would be optimized for a particular type of task. Here, the goal of optimization is to achieve acceptable, not necessarily optimal, performance on all tasks performed (Fig. 10)

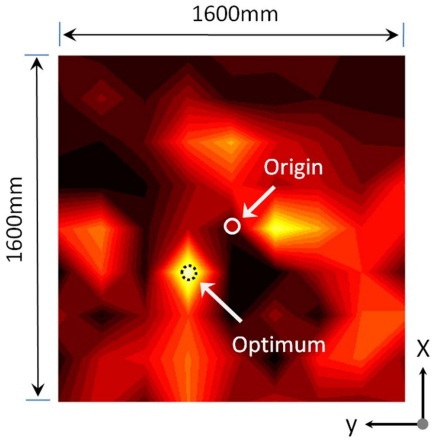

Fig. 9. Optimum manipulator placement for the multitask workspace. Lighter-colored regions represent higher MWGII values.

The data in Table III shows that the multitask optimum placement yields energy consumption and GII comparable to that optimizing over one task. This shows that MWGII-based optimization over several tasks can ensure, if feasible, adequate performance on the entire task set without sacrificing much in individual task performance, providing high task agility. Table IV demonstrates how optimizing placement over only one task increase performance on that task but decreases overall task agility by preventing the completion of, the lowering the quality of, other tasks.

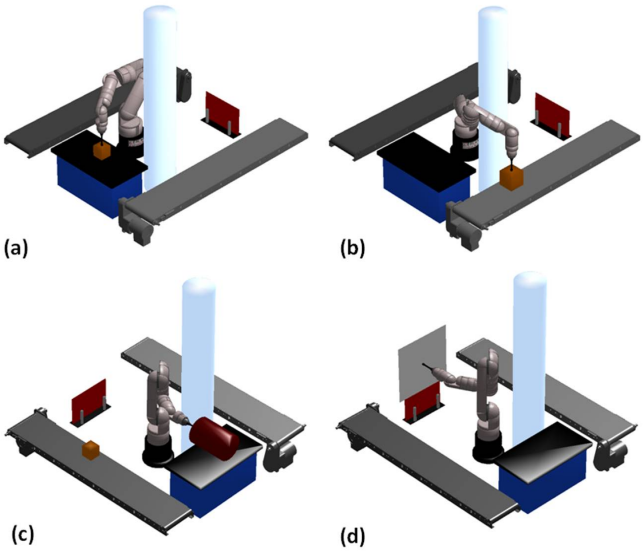

Fig. 10. The manipulator moving (a) a 10kg box, (b) a 20kg box around a support structure, (c) a barrel, and (d) and steel plate, all lifting from the MWGII-based multitask optimal placement.

TABLE III
MULTITASK AND INDIVIDUAL TASK PLACEMENT FITNESS MEASURES

Task Name	MWGII (Multi)	GII (Multi)	GII (Self)	Energy (J) (Multi)	Energy (J) (Self)
10kg Box	0.0244	0.0223	0.0270	802 J	958 J
Barrel Lift	0.0366	0.0520	0.0598	2923 J	3097 J
Steel Plate	0.0283	0.0201	0.0261	1108 J	1246 J
20kg Box	0.0796	0.0899	0.0974	3813 J	3981 J
Multitask	0.0393	0.0455	NA	NA	NA

A comparison of the MWGII, GII, and energy consumption values for the individual task and multitask optimal placements. "Multi" in the column heading means that the values below it correspond to a task performed from the multitask optimum placement, while "Self" means that the values correspond to a task performed from its own the optimum placement.

TABLE IV
THE TASK-SPECIFICITY OF MWGII OPTIMUM PLACEMENT

Task/ Placement	10kg Box	Barrel Lift	Steel Plate	20kg Box	Multi-task
10kg Box	0.0299	0.0210	X	0.0202	0.0244
Barrel Lift	0.0313	0.0329	X	X	0.0366
Steel Plate	X	0.0244	0.0303	0.0124	0.0283
20kg Box	X	0.0751	X	0.0906	0.0796
Multitask	NA	NA	NA	NA	0.0393

A comparison MWGII values, where the table rows are the tasks performed and columns are the task whose optimal placement is used. The X symbols represent a failure to perform a task at a given placement.

Figure 12 shows the optimum placements for individual task optimizations. These plots illustrate the difference in optimum placement location when considering different numbers and types of tasks. Figure 12(b), the MWGII placement map for the barrel task, is very similar to the map of multitask placement. This indicates that the barrel task involves significant motion resistance, probably due to large payload and relatively large reach necessary for completion, and thus has heavy influence on multitask placement.

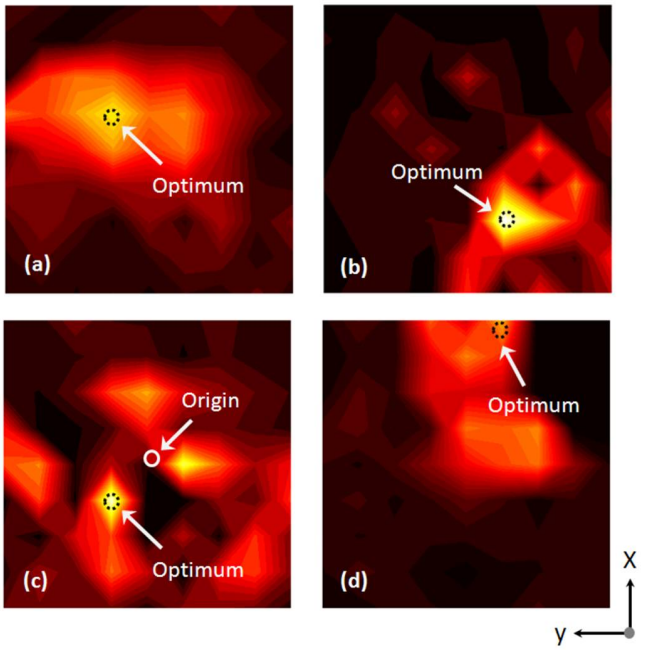

Fig. 11. Optimum placements for the single task workspaces. Here, (a) is the 10kg box task map, (b) is the 20kg box task map, (c) is the barrel task map, and (d) is the steel plate task map. All four maps were normalized with respect to the highest overall MWGII value.

V. Conclusion

The results of this study prove that the multiobjective weighted global isotropy index (MWGII) is an effective tool for determining the optimal placement of a manipulator base in a multitask workspace. By combining the avoidance weighted global isotropy index (AWGII) and the torque weighted global isotropy index (TWGII), we were able to balance adherence to torque limitations, obstacle avoidance, and kinematic isotropy such that a set a four disparate tasks could be completed with adequate timing, reachability, and mechanical advantage. The resulting fitness maps of the candidate placement area show that the MWGII-based fitness measure effectively eliminated all placement coordinates that would cause collisions with the environment as well those areas that require excessive torque and, consequently, exorbitant energy expenditure.

The MWGII is generally a good indication task agility and motion smoothness, but MWGII values do not inherently provide information about the magnitude of end-effector motion possible at a given placement or configuration. In some cases, particularly those where the required motion is always isotropic, magnitude information just is as important, is not more so, than task agility. Experimental studies, using commercially available redundant manipulators, will be conducted in the future to further valid these claims. Future research will be also conducted to develop a method of including both isotropy and motion magnitude in multiobjective performance measures to allow more robust comparisons of design and placement fitness between larger, more variant task sets.

Acknowledgment

We thank Mr. Toshihiko Koyama at DENSO WAVE INCORPORATED for his continued support on this project.. We also thank Professors Matthew Mason and James Kuffner at the Carnegie Mellon Robotics Institute for their manipulator design insights.

References

[1] J, Feddema, "Kinematically Optimal Robot Placement for Minimum Time Coordinated Motion," in *Proc. of the 1996 IEEE Int. Conf. on Robotics and Automation*, Minneapolis, MN, 1996, pp. 3395-3400

[2] T. Yoshikawa, "Manipulability and redundancy control of robotic mechanisms," in *Proc. of the 1985 IEEE Int. Conf. on Robotics and Automation*, Kyoto, Japan, 1985, pp. 1004-1009.

[3] T. Yoshikawa, "Manipulability of Robotic Mechanisms," *The Int. Journal of Robotics Research*, vol. 4, no. 2, pp. 3-9, 1985.

[4] F. Hammond and K. Shimada, "Morphological optimization of kinematically redundant manipulators using weighted isotropy measures," *Proc. of IEEE Int. Conf. on Robotics and Automation*, Kobe, Japan, 2009.

[5] F. Hammond and K. Shimada, "Improvement of Kinematically redundant manipulator design and placement using torque-weighted isotropy measures," *Proc. of Int. Conf. on Advanced Robotics*, Munich, Germany, 2009.

[6] G. Pamanes and S. Zeghloul, "Optimal placement of robotic manipulators using multiple kinematic criteria," *Proc. of IEEE Int. Conf. on Robotics and Automation*, Sacramento, 1991, pp.933-938.

[7] T. C. Lueth, "Automated planning of robot workcell layouts," *Proc. of Int. Conf. on Advanced Robotics*, Nice, Frane, 1992, pp. 1103-1108.

[8] A. P. Pashkevich and M. A. Pashkevich, "Multiobjective optimisation of robot location in a workcell using genetic algorithms." *UKACC Int. Conf. on Control*, Swansea, UK vol. 1, 1998.

[9] D. Hsu, J. C. Latcombe, and S. Sorkin, "Placing a robot manipulator amid obstacles for optimized execution," *Proc. of Int. Symp. On Assembly and Task Planning*, Porto, Portugal 1999, pp. 280-285.

[10] C. A. Klein and B. E. Blaho, "Dexterity Measures for the Design and Control of Kinematically Redundant Manipulators," *The Int. Journal of Robotics Research*, vol. 6, p. 72, 1987.

[11] L. Stocco, S. E. Salcudean, and F. Sassani, "Matrix Normalization for Optimal Robot Design," in *IEEE Int. Conf. on Robotics and Automation*, Leuven, Belgium, 1998, pp. 1346–1351.

[12] W. A. Khan and J. Angeles, "The Kinetostatic Optimization of Robotic Manipulators: The Inverse and the Direct Problems," *Journal of Mechanical Design*, vol. 128, p. 11, January 2006.

[13] M. Tandirci, J. Angeles, and F. Ranjbaran, "The Characteristic Point and the Characteristic Length of Robotic Manipulators," in *Proc. ASME 22nd Biennial Conf. on Robotics, Spatial Mechanisms & Mechanical Systems*, Scotsdale, Arizona, 1992, pp. 203-208.

[14] J. O. Kim and K. Khosla, "Dexterity measures for design and control of manipulators," in *IEEE/RSJ Int. Workshop on Intelligent Robots and Systems*, Osaka, Japan, 1991, pp. 758-763.

[15] A. Maciejewski and C. A. Klein, "Obstacle Avoidance for Kinematically Redundant Manipulators in Dynamically Varying Environments," *The Int. Journal of Robotics Research*, vol. 4, pp.109-117, Fall 1985.

[16] R. Featherstone and D. Orin, "Robot Dynamics : Equations and Algorithms," *Proc. of the 1985 IEEE Int. Conf. on Robotics and Automation*, San Francisco, 2000, pp. 215–221.

[17] S. Ma, "A Stabilized Local Torque Optimization Technique for Redundant Manipulators," *Proc. of the IEEE Int. Conf. On Robotics and Automation*, Nagoya, Japan, 1995, pp. 2791-2796.

[18] C. W. Wampler, "Manipulator inverse kinematic solutions based on vector formulations and damped least-squares methods," *IEEE Trans. on Systems, Man, and Cybernetics*, vol. 16, pp. 93-101, 1986.

[19] M. W. Spong, S. Hutchinson, and M. Vidyasagar, *Robot modeling and control*, Hoboken, NJ: John Wiley & Sons, 2005, pp. 119-161.

[20] T. F. Chan and R. V. Dubey, "A weighted least-norm solution based scheme for avoiding jointlimits for redundant joint manipulators," *IEEE Transactions on Robotics and Automation*, vol. 11, pp. 286-292, April 1995.